Tunable Chiral Bound States with Giant Atoms

Xin Wang,[1,2] Tao Liu,[1] Anton Frisk Kockum,[3] Hong-Rong Li,[2] and Franco Nori[1,4]
[1]Theoretical Quantum Physics Laboratory, RIKEN Cluster for Pioneering Research, Wako-shi, Saitama 351-0198, Japan
[2]MOE Key Laboratory for Nonequilibrium Synthesis and Modulation of Condensed Matter, School of Physics, Xi'an Jiaotong University, 710049 Xi'an, People's Republic of China
[3]Department of Microtechnology and Nanoscience, Chalmers University of Technology, 41296 Gothenburg, Sweden
[4]Physics Department, The University of Michigan, Ann Arbor, Michigan 48109-1040, USA

(Received 21 September 2020; accepted 22 December 2020; published 27 January 2021)

We propose tunable chiral bound states in a system composed of superconducting giant atoms and a Josephson photonic-crystal waveguide (PCW), with no analog in other quantum setups. The chiral bound states arise due to interference in the nonlocal coupling of a giant atom to multiple points of the waveguide. The chirality can be tuned by changing either the atom-waveguide coupling or the external bias of the PCW. Furthermore, the chiral bound states can induce directional dipole-dipole interactions between multiple giant atoms coupling to the same waveguide. Our proposal is ready to be implemented in experiments with superconducting circuits, where it can be used as a tunable toolbox to realize topological phase transitions and quantum simulations.

DOI: 10.1103/PhysRevLett.126.043602

Introduction.—Over the past decades, superconducting quantum circuits (SQCs) have emerged as a powerful platform for quantum information processing [1–9]. For this development, the strong coupling that can be achieved between superconducting qubits (artificial atoms) and microwave photons has played an important role [10–12]. Unlike conventional atom-light interaction, the atomic size in an SQC platform can be comparable to the wavelength of light, indicating that the dipole approximation is no longer valid [13–21]. Such atoms are called superconducting giant atoms. They are nonlocally coupled to multiple points of a waveguide [14,21–27]. Interference effects between these points significantly modify the atom-matter interaction, and, therefore, change the collective behavior of the atoms [14,17,19]. Furthermore, non-Markovian effects, due to time delay of waves propagating between distant coupling points, can play an important role in giant-atom dynamics [16,18,20]. All these exotic phenomena have no counterpart in conventional atom-light systems.

Recently, a number of studies have explored chiral quantum phenomena in waveguide quantum electrodynamics, which enables cascaded quantum circuits, directional qubit interactions, and simulations of many-body physics [28–39]. To achieve these chiral features, many approaches have been proposed for designing unidirectional waveguides, including subwavelength confinement in nanophotonic systems [40–45], spatiotemporal modulation [37], topological engineering [36,46], and structures integrated with synthetic gauge fields [31,47]. The corresponding chiral quantum behavior can emerge via either real propagating photons or virtual nonradiative photons [30–32,36,48]. In particular, chiral quantum systems based on virtual photons can induce directional dipole-dipole interactions between qubits [36], as demonstrated recently in an SQC experiment using a topological waveguide [46]. Experimental realizations of most previous proposals remain elusive in SQCs, so the study of chiral quantum phenomena in SQCs is still in its infancy [39]. Furthermore, the chiral interactions in previous proposals cannot be tuned well, which limits their applications in quantum information processing [49–52].

In this work, we present an alternative tunable chiral quantum system in SQCs. Its directional nature stems from interference effects due to nonlocal coupling of superconducting giant atoms to a Josephson photonic crystal waveguide (PCW). The PCW is constructed by a Josephson-chain metamaterial [53–64], which can be tuned via an external flux bias. The nonlocal coupling of a giant atom to two points of the PCW results in the appearance of chiral bound states whose chiralities can be freely tuned. Tunable chiral many-body interactions of multiple giant atoms is realized through exchange of virtual photons between overlapping such bound states.

Giant-atom-induced tunable chiral bound states.—As shown in Fig. 1, we consider a giant superconducting atom coupled to two points $x_{\pm}$ of a Josephson-chain PCW via capacitances $C_J^{g\pm}$. In contrast to conventional nanophotonic waveguides [65–75], this microwave PCW has a wide range of tunable parameters, including the unit cell length and impedance controlled by the external flux [76–79]. The detailed construction and spectrum of a Josephson PCW can be found in Secs. I and II in the Supplemental Material [80].

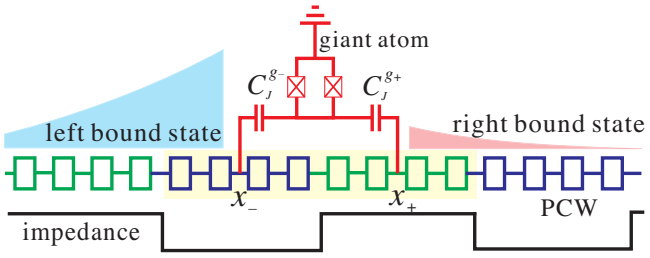

FIG. 1. Sketch of the system. A superconducting giant atom (red) couples via capacitances $C_J^{g\pm}$ to two points $x_\pm$ of a PCW [squares, superconducting quantum interference devices (SQUIDs)]. The green (blue) SQUIDs denote high (low) impedance. In our work, we assume the periodic impedance modulation as a cosine wave. The results remain robust when we consider other shapes of modulation signals (e.g., a square wave) [80]. The points x_+ and x_- are assumed to be within one period of the modulation (yellow area). The left (right) photonic component of a bound state is shown in blue (red).

When the atomic transition frequency ω_q is in the PCW band gap, and close to the top of the lowest energy band ω_k in the first Brillouin zone (BZ), the interaction Hamiltonian is

$$H_{\rm int} = \sum_{k\in \rm BZ} \hbar\Delta_k a_k^\dagger a_k + \sum_{k\in \rm BZ} \hbar(g_k a_k^\dagger \sigma_- + g_k^* a_k \sigma_+), \quad (1)$$

where $\Delta_k = \omega_k - \omega_q$ is the frequency detuning, $\sigma_\pm$ are the atom raising and lowering operators, a_k ($a_k^\dagger$) is the annihilation (creation) operator of the photonic mode with wave vector k in the lowest energy band, and the nonlocal atom-waveguide coupling strength is given by (see Sec. III in the Supplemental Material [80])

$$g_k = \sum_{i=\pm} g_k^i e^{ikx_i} u_k(x_i), \quad \text{with} \quad g_k^\pm \simeq \frac{e}{\hbar}\frac{C_J^{g\pm}}{C_\Sigma}\sqrt{\frac{\hbar\omega_q}{C_t}}. \quad (2)$$

Here C_Σ (C_t) is the total capacitance of the atom (PCW), and $u_k(x) = u_k(x+\lambda_m)$ is the Bloch wave function with a tunable modulating wavelength λ_m of the PCW. We compute $u_k(x)$ and g_k numerically based on experimental values of the SQUID-chain PCWs in Refs. [59,61,63].

We find the bound state of the system by solving $H_{\rm int}|\psi_b\rangle = \hbar\epsilon_b|\psi_b\rangle$, with eigenenergy ϵ_b and eigenstate $|\psi_b\rangle = \cos(\theta)|e,0\rangle + \sin(\theta)\sum_k c_k|g,1_k\rangle$, in the single-excitation subspace. Previous studies of small atoms in waveguides [68–74], and one on giant atoms in an coupled-resonator waveguide [85], have shown that the bound state decays exponentially and symmetrically in both directions.

For the case of a giant atom, the real-space wave function of the photonic component of the bound state is approximated by (see Sec. IV in Ref. [80])

$$\phi_b(x) = \sin(\theta)\langle x|\sum_k c_k a_k^\dagger|0\rangle = \sum_{i=\pm}\phi_b^i(x), \quad (3)$$

with

$$\phi_b^i(x) \propto \int \frac{g_k^i u_k(x_i)u_k^*(x)e^{-ik(x-x_i)}}{\epsilon_b - \Delta_k}dk = A^i(x)e^{i\theta_i(x)}, \quad (4)$$

where $\phi_b^\pm(x)$ represent the photonic wave function components of the bound state for a small atom coupling at positions $x_\pm$; $A^\pm$ and $\theta_\pm$ denote their corresponding amplitudes and phases, respectively. The phases of atom-waveguide coupling amplitudes [see Eq. (2)] at positions x_+ and x_- cannot be simultaneously gauged out due to the nonlocal coupling. This results in interference between $\phi_b^+(x)$ and $\phi_b^-(x)$ [see Eqs. (3) and (4)], leading to the formation of a chiral bound state.

As depicted in Fig. 1, we assume the PCW to be infinitely long in both directions, and the original point $x = 0$ at the middle of the low-impedance part in one cell. The giant-atom coupling points x_- and x_+ are located at $\{x_-, x_+\} = \{0, 0.5\lambda_m\}$. We find that the bound-state components $\phi_b^\pm(x)$ distribute symmetrically around the coupling points [80]. However, as depicted in Fig. 2(a), their phase difference is $\delta\theta = \theta_+ - \theta_- \simeq 0$ for $x \ll x_-$, while it is $\delta\theta \simeq \pi$ for $x \gg x_+$. Numerical results indicate that maximum interference is achieved when $g_k^+ \simeq 3.4 g_k^-$, giving $A^+(x) \simeq A^-(x)$. Consequently, the right (left) bound state vanishes (is maximally enhanced) due to destructive (constructive) interference. Figure 2(b) shows the real-space distribution of $\phi_b(x)$, which is strongly localized to the left of the giant atom. Note that, for other positions of the coupling points, there exist different interference patterns between $\phi_b^\pm(x)$, which lead to different chirality. Detailed discussions can be found in Sec. IV in the Supplemental Material [80].

The chiral bound state can be phenomenologically interpreted as a result of interference, as explained above. We now make a quantitative analysis. When a small atom is coupled to a PCW, as studied in Refs. [71–75], the atom-

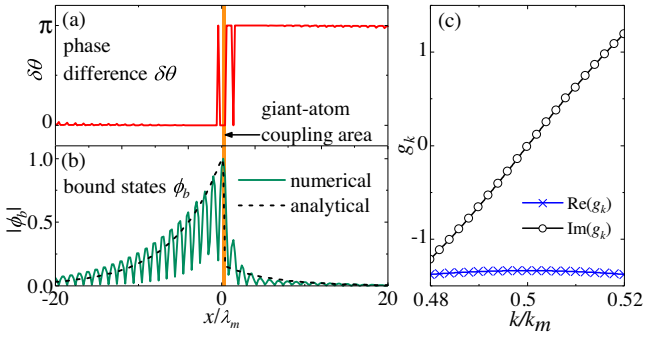

FIG. 2. Properties of a chiral bound state. (a) Phase differences between $\phi_b^+(x)$ and $\phi_b^-(x)$ versus of x for $\{x_-, x_+\} = \{0, 0.5\lambda_m\}$. (b) The bound state amplitude $|\phi_b(x)|$ for the same setup. The solid (dashed) curve is the numerical (analytical) result described by Eq. (4) [Eq. (6)]. (c) The imaginary and real part of g_k versus k for the same setup.

waveguide coupling amplitude g_k is a constant independent of the wave vector k, i.e., $g_k \simeq g_{k_0}$, with $k_0 = k_m/2$, and $k_m = 2\pi/\lambda_m$. The giant-atom case is different, as shown in Fig. 2(c), where we plot the real and imaginary parts of g_k versus k. Note that, around k_0, the real part of g_k is approximately constant, but the imaginary part changes linearly with k. We therefore rewrite g_k as

$$g_k \simeq (A + iB\delta k), \tag{5}$$

where $\delta k = k - k_0$, A represents the average real part of g_k around k_0, and B is the slope of the imaginary part of g_k. Because of the nonlocal coupling of the giant atom to the PCW, B has a nonzero value, and cannot be gauged out. In addition, by considering the effective-mass approximation [70,71], the dispersion relation of the lowest energy band of the PCW around the band edge can be expressed as $\Delta_k = -\delta_0 - \alpha_m(k - k_0)^2$ (see Sec. III in Ref. [80]), and $\phi_b(x)$ in Eq. (3) becomes

$$\phi_b(x) \propto [C_-\Theta(-x) + C_+\Theta(x)] \exp\left(-\frac{|x|}{L_{\text{eff}}}\right), \tag{6}$$

where $L_{\text{eff}} = \sqrt{\alpha_m/\delta_0}$ is the decay length, $\Theta(x)$ is the Heaviside step function, and $C_\pm$ are determined by the imaginary and real parts of g_k as

$$C_\pm = A \pm B\sqrt{\frac{\delta_0}{\alpha_m}}. \tag{7}$$

In Eq. (6), we have assumed $|x_+ - x_-| < \lambda_m \ll L_{\text{eff}}$. This approximation holds in Fig. 2(b), where the photonic component between the two coupling points (brown area) is much smaller than the left and right parts, and can be neglected. Therefore, when considering the bound-state distribution, we view $x_\pm$ as both approximately being at $x = 0$. For the parameters used in Fig. 2, we have $|C_-| \gg |C_+|$. Consequently, the photonic component of the bound state mostly distributes to the left of the giant atom. Note that the above analytical results fit well with the numerical ones, as shown in Fig. 2(b).

We now define the chirality of the bound state as

$$\mathcal{C}_b = \frac{\Phi_L - \Phi_R}{\Phi_L + \Phi_R}, \qquad \Phi_{R/L} = \left| \int_{\pm\infty}^{x_\pm} |\phi_b(x')|^2 dx' \right|, \tag{8}$$

where the chiral preferred direction is left (right) given that $\mathcal{C}_b > 0$ ($\mathcal{C}_b < 0$), and $\mathcal{C}_b \to 1$ ($\mathcal{C}_b \to -1$) indicates perfect left (right) chirality. Using Eq. (6), the analytical form of $\mathcal{C}_b$ becomes

$$\mathcal{C}_b = \frac{C_-^2 - C_+^2}{C_-^2 + C_+^2}. \tag{9}$$

In Fig. 3(a), we plot both the numerical and analytical $\mathcal{C}_b$ versus x_+ by fixing $x_- = 0$ and $g_k^+ = g_k^-$. The numerical

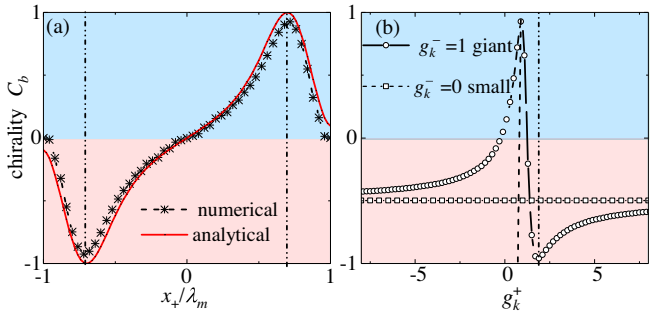

FIG. 3. Tuning the chirality of the bound state. (a) Chirality $\mathcal{C}_b$ versus x_+ for fixed $x_- = 0$ and $g_k^+ = g_k^-$. The dashed lines indicate the maximum chirality $|\mathcal{C}_b| \simeq 1$. (b) Chirality versus g_k^+ for fixed $\{x_-, x_+\} = \{0, 0.75\lambda_m\}$ and $g_k^- = 1$ (giant-atom case) or $g_k^- = 0$ (small-atom case).

parameters of the whole system are adopted from the experiments in Refs. [59,61,63] (see Sec. III in the Supplemental Material [80]). The sign of $\mathcal{C}_b$ changes when the second coupling point x_+ is moved from the left side of x_- to the right side. At $x_+/\lambda_m \simeq \pm 0.7$ [dashed lines in Fig. 3(a)], the chirality reaches its maximum value $|\mathcal{C}_b| \simeq 0.95$. In Fig. 3(b), we fix $\{x_-, x_+\} = \{0, 0.75\lambda_m\}$ and plot $\mathcal{C}_b$ versus the coupling strength g_k^+. The results in Fig. 3 show that the chirality can be continuously tuned over the whole range $\mathcal{C}_b \in (-1, 1)$ by changing either x_+ or g_k^+.

Unlike the case of nanophotonic waveguide quantum electrodynamics [68,75], an atom placed in the PCW can see different semi-infinite waveguide structures to the right and left of a coupling point. This symmetry breaking is what enables chirality. As shown in Fig. 3(b), the symmetry breaking enables the formation of a chiral bound state not only with a giant atom, but also with a small atom, which has not been explored in previous studies. For $|g_k^+| \gg |g_k^-|$, which corresponds to the small-atom case, we find $\mathcal{C}_b \simeq -0.49$ when $\{x_-, x_+\} = \{0, 0.75\lambda_m\}$. However, the chirality for a small atom is never perfect ($|\mathcal{C}_b| < 1$) and cannot be tuned by changing the coupling strength, in contrast to the giant-atom case [Fig. 3(b)]. Additionally, $\mathcal{C}_b$ is quite sensitive to the coupling position. A detailed discussion is provided in the Supplemental Material [80].

Chiral dipole-dipole interactions.—When multiple small atoms are coupled within the band gap of the same PCW, effective dipole-dipole interactions between them are induced through the exchange of virtual photons in the PCW. The interaction strength is determined by the overlap between the decaying evanescent fields of the bound states [69–75]. In previous studies with cold-atom systems [71,75], where the atoms are equally spaced, the nearest-neighbor interaction strength is constant. For the chiral bound states induced by the coupling between a PCW and giant atoms, the scenario is different.

As shown in Fig. 4, we consider giant atoms A and B equally distributed along a PCW with an interatom distance D_q. Here, the PCW impedance modulation is simplified as

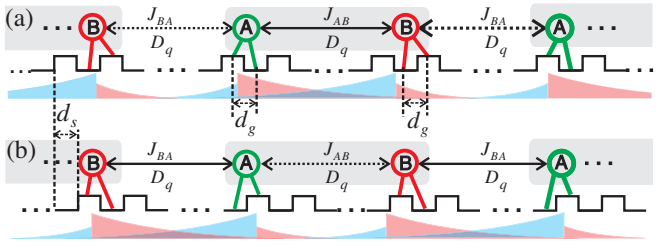

FIG. 4. Setups for chiral dipole-dipole interactions betweeen giant atoms. (a) Giant atoms A and B, separated by a distance D_q, coupled to a Josephson-chain PCW. The periodic impedance modulation is a square wave. The induced effective dipole-dipole coupling is chiral with $J_{AB} \gg J_{BA}$. (b) Relative to (a), the impedance modulation signal is shifted with a distance $d_s = 0.5\lambda_m$. The bound-state chiralities are reversed, resulting in $J_{AB} \ll J_{BA}$.

square waves. One leg of each giant atom A and B is coupled to the low-impedance points $x_-^{A,B}$. while the second coupling points $x_+^{A,B}$ are placed either to the left or to the right (different for A and B) of $x_-^{A,B}$ at the closest high-impedance position. Therefore, the bound states of giant atoms A and B satisfy $\mathcal{C}_b^A = -\mathcal{C}_b^B$. The atomic pair $\{A, B\}$ is repeated along the PCW, and can be viewed as a dimer (see Fig. 4). The intracell dipole-dipole interaction can be derived via standard resolvent-operator techniques [80,86,87]:

$$\mathrm{Re}[\Sigma_{AB}(z)] = \mathrm{Re}\left[\int_0^{k_0} dk \frac{2\mathrm{Re}(g_{kA}g_{kB}^*)}{z - \Delta_k}\right] \simeq J_{AB}, \quad (10)$$

where the real part J_{AB} of $\Sigma_{AB}(z)$ describes the coherent dipole-dipole coupling between intracell atoms. The atomic decay effects can be strongly suppressed with a large detuning δ_0 [31,36,87] (see Sec. V in the Supplemental Material [80]). The intercell coupling amplitude J_{BA} can be found similarly.

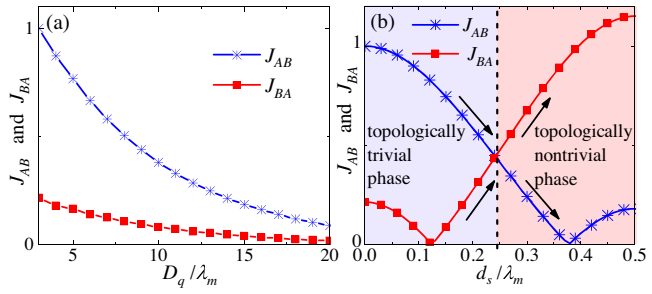

FIG. 5. Chiral interaction and topological phase transition. (a) Dipole-dipole interaction strengths J_{AB} and J_{BA} (normalized by J_{AB} at $D_q = 3\lambda_m$) versus separation D_q. (b) J_{AB} and J_{BA} for fixed D_q versus of the shift distance d_s [relative to Fig. 4(a)] for the PCW impedance modulation. As the shift distance is increased towards $d_s = 0.5\lambda_m$, the chiral interaction strengths of J_{AB} and J_{BA} are exchanged, leading to a topological phase transition.

In Fig. 5(a), we numerically plot J_{AB} and J_{BA}, both of which exponentially decay with D_q [69–73], for the setup in Fig. 4(a). Since the bound-state chiralities of A and B are opposite, the decaying evanescent fields within a unit cell have much larger overlap than those between different cells. This leads to a much larger intracell dipole-dipole interaction J_{AB} than the intercell interaction J_{BA}, i.e., the interaction is *chiral* even though the giant atoms are equally spaced. Since the bound states of A and B can be tuned to $|\mathcal{C}_b| \simeq 1$, the atoms only interact with the atoms in their chiral preferred directions, but cannot interact with those in the opposite direction, no matter how small the separation D_q is.

Topological phases with giant atoms.—The impedance of the Josephson PCW can be modulated via an external flux bias [80]. As shown in Fig. 4, shifting the programmable modulation signal by d_s, the high-impedance positions will be moved [80]. For $d_s = 0.5\lambda_m$, the chiralities of the giant atoms in Fig. 4 are switched, leading to $J_{AB} \ll J_{BA}$. Figure. 5(b) shows that J_{AB} (J_{BA}) decreases (increases) linearly with d_s around $d_s \simeq 0.25\lambda_m$.

By modulating d_s in time, we can simulate topological phases. We assume that the frequency of each atom is also modulated in time [5]. As shown in Fig. 4, after tracing out the PCW, we map the atomic-chain Hamiltonian to the Su-Schrieffer-Heeger model

$$H_{\mathrm{qc}} = \sum_i [J_{AB}(t)\sigma_{Ai}^- \sigma_{Bi}^+ + J_{BA}(t)\sigma_{Bi}^- \sigma_{Ai+1}^+ + \mathrm{H.c.}] + \sum_i \Delta_q(t)(\sigma_{Ai}^z - \sigma_{Bi}^z), \quad (11)$$

where $\Delta_q(t)$ is the frequency detuning between atoms A and B. The degeneracy point of the chain is at $\{J_{BA} - J_{AB}, \Delta_q\} = \{0, 0\}$ [80]. The adiabatic Thouless pump trajectories (see Fig. 6), which encircle the degeneracy point, are topologically equivalent, and robust to disorders and perturbations [88–90]. As shown in Fig. 5(b), for $d_s \simeq 0.25\lambda_m$, the bound states of atom A and B, do not show any chirality, leading to $J_{AB} - J_{BA} = 0$. This corresponds to the topological phase transition point [91–93].

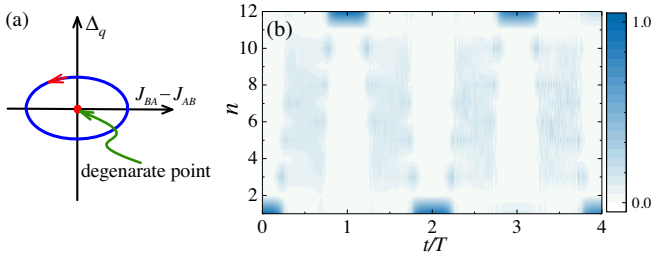

FIG. 6. Topological protection. (a) The pump circle in parameter space $\{J_{BA} - J_{AB}, \Delta_q\}$. The topologically nontrivial pumping corresponds to a closed path encircling the degeneracy point at the origin. (b) Time evolution of a single excitation in the atomic chain (with 12 sites) under adiabatic pumping loops (see Sec. V in Ref. [80]).

In Fig. 6(b), we plot the adiabatic pumping process for the evolution of an initial excitation localized at the left edge of the atomic chain (see Sec. V in the Supplemental Material [80]). At the end of each pump circle, the excitation is transferred to the right edge state with a high fidelity due to topological protection [88]. This process exploits the directional interactions between giant atoms, and just needs to shift the modulation signal by a small length, which is feasible in SQC platforms.

Conclusion.—In this work, we have explored giant superconducting atoms coupled to two points of a Josephson-chain PCW. We showed that interference arising due to the nonlocal coupling leads to chiral bound states. The chirality of these states can be easily tuned over the full range by either modulating the external flux bias of the PCW or changing the coupling strengths. For multiple giant atoms equally spaced along the waveguide, the dipole-dipole interactions exhibit strong chirality due to spatially asymmetric overlaps between the bound states. Each atom can be tuned to only interact with atoms in a preferred direction. Using this chiral interaction, we demonstrated that our proposal can realize a topological phase transition and topological Thouless pumping. Extending our setup to 2D PCWs might lead to more exotic quantum phenomena. We hope that our proposal can be a powerful toolbox to achieve chiral long-range interactions for quantum simulations and many-body physics. The setups we have studied here can be realized in experiments using currently available state-of-the-art technology for superconducting circuits.

X. W. is supported by the China Postdoctoral Science Foundation No. 2018M631136 and the Natural Science Foundation of China under Grant No. 11804270. A. F. K. acknowledges support from the Japan Society for the Promotion of Science (BRIDGE Fellowship BR190501), the Swedish Research Council (Grant No. 2019-03696), and the Knut and Alice Wallenberg Foundation through the Wallenberg Centre for Quantum Technology (WACQT). H. R. L. is supported by the National Science Foundation of China (Grant No. 11774284). F. N. is supported in part by NTT Research, Army Research Office (ARO) (Grant No. W911NF-18-1-0358), Japan Science and Technology Agency (JST) (via the Q-LEAP program and CREST Grant No. JPMJCR1676), Japan Society for the Promotion of Science (JSPS) (via the KAKENHI Grant No. JP20H00134 and the JSPS-RFBR Grant No. JPJSBP120194828), the Asian Office of Aerospace Research and Development (AOARD), and the Foundational Questions Institute Fund (FQXi) via Grant No. FQXi-IAF19-06.

[1] J. Q. You and F. Nori, Quantum information processing with superconducting qubits in a microwave field, Phys. Rev. B **68**, 064509 (2003).

[2] J. Koch, T. M. Yu, J. Gambetta, A. A. Houck, D. I. Schuster, J. Majer, A. Blais, M. H. Devoret, S. M. Girvin, and R. J. Schoelkopf, Charge-insensitive qubit design derived from the Cooper pair box, Phys. Rev. A **76**, 042319 (2007).

[3] J. Q. You and F. Nori, Superconducting circuits and quantum information, Phys. Today **58**, No. 11, 42 (2005).

[4] J. Clarke and F. K. Wilhelm, Superconducting quantum bits, Nature (London) **453**, 1031 (2008).

[5] X. Gu, A. F. Kockum, A. Miranowicz, Y.-X. Liu, and F. Nori, Microwave photonics with superconducting quantum circuits, Phys. Rep. **718–719**, 1 (2017).

[6] C. Song, J. Cui, H. Wang, J. Hao, H. Feng, and Y. Li, Quantum computation with universal error mitigation on a superconducting quantum processor, Sci. Adv. **5**, eaaw5686 (2019).

[7] F. Arute *et al.*, Quantum supremacy using a programmable superconducting processor, Nature (London) **574**, 505 (2019).

[8] A. F. Kockum and F. Nori, Quantum bits with Josephson junctions, in *Fundamentals and Frontiers of the Josephson Effect*, edited by F. Tafuri (Springer, New York, 2019), pp. 703–741.

[9] M. Kjaergaard, M. E. Schwartz, J. Braumüller, P. Krantz, J. I.-J. Wang, S. Gustavsson, and W. D. Oliver, Superconducting qubits: Current state of play, Annu. Rev. Condens. Matter Phys. **11**, 369 (2020).

[10] A. Wallraff, D. I. Schuster, A. Blais, L. Frunzio, R.-S. Huang, J. Majer, S. Kumar, S. M. Girvin, and R. J. Schoelkopf, Strong coupling of a single photon to a superconducting qubit using circuit quantum electrodynamics, Nature (London) **431**, 162 (2004).

[11] T. Niemczyk, F. Deppe, H. Huebl, E. P. Menzel, F. Hocke, M. J. Schwarz, J. J. Garcia-Ripoll, D. Zueco, T. Hümmer, E. Solano, A. Marx, and R. Gross, Circuit quantum electrodynamics in the ultrastrong-coupling regime, Nat. Phys. **6**, 772 (2010).

[12] A. F. Kockum, A. Miranowicz, S. De Liberato, S. Savasta, and F. Nori, Ultrastrong coupling between light and matter, Nat. Rev. Phys. **1**, 19 (2019).

[13] M. V. Gustafsson, T. Aref, A. F. Kockum, M. K. Ekström, G. Johansson, and P. Delsing, Propagating phonons coupled to an artificial atom, Science **346**, 207 (2014).

[14] A. F. Kockum, P. Delsing, and G. Johansson, Designing frequency-dependent relaxation rates and Lamb shifts for a giant artificial atom, Phys. Rev. A **90**, 013837 (2014).

[15] T. Aref, P. Delsing, M. K. Ekström, A. F. Kockum, M. V. Gustafsson, G. Johansson, P. J. Leek, E. Magnusson, and R. Manenti, Quantum acoustics with surface acoustic waves, in *Superconducting Devices in Quantum Optics*, edited by R. H. Hadfield and G. Johansson (Springer, New York, 2016).

[16] L. Guo, A. L. Grimsmo, A. F. Kockum, M. Pletyukhov, and G. Johansson, Giant acoustic atom: A single quantum system with a deterministic time delay, Phys. Rev. A **95**, 053821 (2017).

[17] A. F. Kockum, G. Johansson, and F. Nori, Decoherence-Free Interaction between Giant Atoms in Waveguide Quantum Electrodynamics, Phys. Rev. Lett. **120**, 140404 (2018).

[18] G. Andersson, B. Suri, L.-Z. Guo, T. Aref, and P. Delsing, Non-exponential decay of a giant artificial atom, Nat. Phys. **15**, 1123 (2019).

[19] A. F. Kockum, Quantum optics with giant atoms—the first five years, in *International Symposium on Mathematics, Quantum Theory, and Cryptography* (Springer Singapore, Singapore, 2021), p. 125.

[20] L.-Z. Guo, A. F. Kockum, F. Marquardt, and G. Johansson, Oscillating bound states for a giant atom, Phys. Rev. Research **2**, 043014 (2020).

[21] B. Kannan, M. J. Ruckriegel, D. L. Campbell, A. F. Kockum, J. Braumüller, D. K. Kim, M. Kjaergaard, P. Krantz, A. Melville, B. M. Niedzielski, A. Vepsäläinen, R. Winik, J. L. Yoder, F. Nori, T. P. Orlando, S. Gustavsson, and W. D. Oliver, Waveguide quantum electrodynamics with superconducting artificial giant atoms, Nature (London) **583**, 775 (2020).

[22] R. Manenti, A. F. Kockum, A. Patterson, T. Behrle, J. Rahamim, G. Tancredi, F. Nori, and P. J. Leek, Circuit quantum acoustodynamics with surface acoustic waves, Nat. Commun. **8**, 975 (2017).

[23] P. Delsing *et al.*, The 2019 surface acoustic waves roadmap, J. Phys. D **52**, 353001 (2019).

[24] L. R. Sletten, B. A. Moores, J. J. Viennot, and K. W. Lehnert, Resolving Phonon Fock States in a Multimode Cavity with a Double-Slit Qubit, Phys. Rev. X **9**, 021056 (2019).

[25] A. M. Vadiraj, A. Ask, T. G. McConkey, I. Nsanzineza, C. W. Sandbo Chang, A. F. Kockum, and C. M. Wilson, Engineering the level structure of a giant artificial atom in waveguide quantum electrodynamics, arXiv:2003.14167.

[26] G. Andersson, M. K. Ekström, and P. Delsing, Electromagnetically Induced Acoustic Transparency with a Superconducting Circuit, Phys. Rev. Lett. **124**, 240402 (2020).

[27] A. Bienfait, Y. P. Zhong, H.-S. Chang, M.-H. Chou, C. R. Conner, É. Dumur, J. Grebel, G. A. Peairs, R. G. Povey, K. J. Satzinger, and A. N. Cleland, Quantum Erasure Using Entangled Surface Acoustic Phonons, Phys. Rev. X **10**, 021055 (2020).

[28] H. J. Carmichael, Quantum Trajectory Theory for Cascaded Open Systems, Phys. Rev. Lett. **70**, 2273 (1993).

[29] C. W. Gardiner, Driving a Quantum System with the Output Field from Another Driven Quantum System, Phys. Rev. Lett. **70**, 2269 (1993).

[30] H. Pichler, T. Ramos, A. J. Daley, and P. Zoller, Quantum optics of chiral spin networks, Phys. Rev. A **91**, 042116 (2015).

[31] T. Ramos, B. Vermersch, P. Hauke, H. Pichler, and P. Zoller, Non-Markovian dynamics in chiral quantum networks with spins and photons, Phys. Rev. A **93**, 062104 (2016).

[32] P. Lodahl, S. Mahmoodian, S. Stobbe, A. Rauschenbeutel, P. Schneeweiss, J. Volz, H. Pichler, and P. Zoller, Chiral quantum optics, Nature (London) **541**, 473 (2017).

[33] B. Vermersch, P.-O. Guimond, H. Pichler, and P. Zoller, Quantum State Transfer via Noisy Photonic and Phononic Waveguides, Phys. Rev. Lett. **118**, 133601 (2017).

[34] Z.-L. Xiang, M.-Z. Zhang, L. Jiang, and P. Rabl, Intracity Quantum Communication via Thermal Microwave Networks, Phys. Rev. X **7**, 011035 (2017).

[35] A. Grankin, P. O. Guimond, D. V. Vasilyev, B. Vermersch, and P. Zoller, Free-space photonic quantum link and chiral quantum optics, Phys. Rev. A **98**, 043825 (2018).

[36] M. Bello, G. Platero, J. I. Cirac, and A. González-Tudela, Unconventional quantum optics in topological waveguide QED, Sci. Adv. **5**, eaaw0297 (2019).

[37] G. Calajó, M. J. A. Schuetz, H. Pichler, M. D. Lukin, P. Schneeweiss, J. Volz, and P. Rabl, Quantum acousto-optic control of light-matter interactions in nanophotonic networks, Phys. Rev. A **99**, 053852 (2019).

[38] K. Y. Bliokh, D. Leykam, M. Lein, and F. Nori, Topological non-Hermitian origin of surface maxwell waves, Nat. Commun. **10**, 580 (2019).

[39] P. O. Guimond, B. Vermersch, M. L. Juan, A. Sharafiev, G. Kirchmair, and P. Zoller, A unidirectional on-chip photonic interface for superconducting circuits, npj Quantum Inf. **6**, 32 (2020).

[40] R. Mitsch, C. Sayrin, B. Albrecht, P. Schneeweiss, and A. Rauschenbeutel, Quantum state-controlled directional spontaneous emission of photons into a nanophotonic waveguide, Nat. Commun. **5**, 5713 (2014).

[41] K. Y. Bliokh, D. Smirnova, and F. Nori, Quantum spin Hall effect of light, Science **348**, 1448 (2015).

[42] J. Petersen, J. Volz, and A. Rauschenbeutel, Chiral nanophotonic waveguide interface based on spin-orbit interaction of light, Science **346**, 67 (2014).

[43] A. B. Young, A. C. T. Thijssen, D. M. Beggs, P. Androvitsaneas, L. Kuipers, J. G. Rarity, S. Hughes, and R. Oulton, Polarization Engineering in Photonic Crystal Waveguides for Spin-Photon Entanglers, Phys. Rev. Lett. **115**, 153901 (2015).

[44] K. Y. Bliokh and F. Nori, Transverse and longitudinal angular momenta of light, Phys. Rep. **592**, 1 (2015).

[45] K. Y. Bliokh, F. J. Rodríguez-Fortuño, F. Nori, and A. V. Zayats, Spin–orbit interactions of light, Nat. Photonics **9**, 796 (2015).

[46] E.-J. Kim, X.-Y. Zhang, V. S. Ferreira, J. Banker, J. K. Iverson, A. Sipahigil, M. Bello, A. Gonzalez-Tudela, M. Mirhosseini, and O. Painter, Quantum electrodynamics in a topological waveguide, arXiv:2005.03802 [Phys. Rev. X (to be published)].

[47] E. Sánchez-Burillo, C. Wan, D. Zueco, and A. González-Tudela, Chiral quantum optics in photonic sawtooth lattices, Phys. Rev. Research **2**, 023003 (2020).

[48] L. Leonforte, A. Carollo, and F. Ciccarello, Vacancy-like dressed states in topological waveguide QED, arXiv:2007.02949.

[49] J.-Q. Liao, Z. R. Gong, L. Zhou, Y.-X. Liu, C. P. Sun, and F. Nori, Controlling the transport of single photons by tuning the frequency of either one or two cavities in an array of coupled cavities, Phys. Rev. A **81**, 042304 (2010).

[50] Y. B. Liu and A. A. Houck, Quantum electrodynamics near a photonic bandgap, Nat. Phys. **13**, 48 (2017).

[51] N. M. Sundaresan, R. Lundgren, G.-Y. Zhu, A. V. Gorshkov, and A. A. Houck, Interacting Qubit-Photon Bound States with Superconducting Circuits, Phys. Rev. X **9**, 011021 (2019).

[52] I. Carusotto, A. A. Houck, A. J. Kollar, P. Roushan, D. I. Schuster, and J. Simon, Photonic materials in circuit quantum electrodynamics, Nat. Phys. **16**, 268 (2020).

[53] A. L. Rakhmanov, A. M. Zagoskin, S. Savel'ev, and F. Nori, Quantum metamaterials: Electromagnetic waves in a Josephson qubit line, Phys. Rev. B **77**, 144507 (2008).

[54] M. Leib, F. Deppe, A. Marx, R. Gross, and M. J. Hartmann, Networks of nonlinear superconducting transmission line resonators, New J. Phys. **14**, 075024 (2012).
[55] N. A. Masluk, I. M. Pop, A. Kamal, Z. K. Minev, and M. H. Devoret, Microwave Characterization of Josephson Junction Arrays: Implementing a Low Loss Superinductance, Phys. Rev. Lett. **109**, 137002 (2012).
[56] C. Altimiras, O. Parlavecchio, P. Joyez, D. Vion, P. Roche, D. Esteve, and F. Portier, Tunable microwave impedance matching to a high impedance source using a Josephson metamaterial, Appl. Phys. Lett. **103**, 212601 (2013).
[57] G. Rastelli and I. M. Pop, Tunable ohmic environment using Josephson junction chains, Phys. Rev. B **97**, 205429 (2018).
[58] T. Weißl, B. Küng, E. Dumur, A. K. Feofanov, I. Matei, C. Naud, O. Buisson, F. W. J. Hekking, and W. Guichard, Kerr coefficients of plasma resonances in Josephson junction chains, Phys. Rev. B **92**, 104508 (2015).
[59] Y. Krupko, V. D. Nguyen, T. Weißl, É. Dumur, J. Puertas, R. Dassonneville, C. Naud, F. W. J. Hekking, D. M. Basko, O. Buisson, N. Roch, and W. Hasch-Guichard, Kerr nonlinearity in a superconducting Josephson metamaterial, Phys. Rev. B **98**, 094516 (2018).
[60] M. Mirhosseini, E. Kim, V. S. Ferreira, M. Kalaee, A. Sipahigil, A. J. Keller, and O. Painter, Superconducting metamaterials for waveguide quantum electrodynamics, Nat. Commun. **9**, 3706 (2018).
[61] T. Weissl, Quantum phase and charge in Josephson junction chains, Ph.D. thesis, Grenoble, 2014.
[62] S. Karkar, E. De Bono, M. Collet, G. Matten, M. Ouisse, and E. Rivet, Broadband Nonreciprocal Acoustic Propagation Using Programmable Boundary Conditions: From Analytical Modeling to Experimental Implementation, Phys. Rev. Applied **12**, 054033 (2019).
[63] J. P. Martínez, S. Léger, N. Gheeraert, R. Dassonneville, L. Planat, F. Foroughi, Y. Krupko, O. Buisson, C. Naud, W. Hasch-Guichard, S. Florens, I. Snyman, and N. Roch, A tunable Josephson platform to explore many-body quantum optics in circuit-QED, npj Quantum Inf. **5**, 19 (2019).
[64] L. Planat, A. Ranadive, R. Dassonneville, J. M. Puertas, S. Léger, C. Naud, O. Buisson, W. Hasch-Guichard, D. M. Basko, and N. Roch, Photonic-Crystal Josephson Traveling-Wave Parametric Amplifier, Phys. Rev. X **10**, 021021 (2020).
[65] S. John and J. Wang, Quantum Electrodynamics near a Photonic Band Gap: Photon Bound States and Dressed Atoms, Phys. Rev. Lett. **64**, 2418 (1990).
[66] L. Zhou, H. Dong, Y.-X. Liu, C. P. Sun, and F. Nori, Quantum supercavity with atomic mirrors, Phys. Rev. A **78**, 063827 (2008).
[67] S. John and J. Wang, Quantum optics of localized light in a photonic band gap, Phys. Rev. B **43**, 12772 (1991).
[68] C.-L. Hung, S. M. Meenehan, D. E. Chang, O. Painter, and H. J. Kimble, Trapped atoms in one-dimensional photonic crystals, New J. Phys. **15**, 083026 (2013).
[69] A. Goban, C.-L. Hung, S.-P. Yu, J. Hood, J. Muniz, J. Lee, M. Martin, A. McClung, K. Choi, D. Chang, O. Painter, and H. Kimble, Atom–light interactions in photonic crystals, Nat. Commun. **5**, 3808 (2014).
[70] A. González-Tudela, C.-L. Hung, D. E. Chang, J. I. Cirac, and H. J. Kimble, Subwavelength vacuum lattices and atom–atom interactions in two-dimensional photonic crystals, Nat. Photonics **9**, 320 (2015).
[71] J. S. Douglas, H. Habibian, C.-L. Hung, A. V. Gorshkov, H. J. Kimble, and D. E. Chang, Quantum many-body models with cold atoms coupled to photonic crystals, Nat. Photonics **9**, 326 (2015).
[72] J. D. Hood, A. Goban, A. Asenjo-Garcia, M. Lu, S.-P. Yu, D. E. Chang, and H. J. Kimble, Atom–atom interactions around the band edge of a photonic crystal waveguide, Proc. Natl. Acad. Sci. U.S.A. **113**, 10507 (2016).
[73] J. S. Douglas, T. Caneva, and D. E. Chang, Photon Molecules in Atomic Gases Trapped Near Photonic Crystal Waveguides, Phys. Rev. X **6**, 031017 (2016).
[74] E. Munro, L. C. Kwek, and D. E. Chang, Optical properties of an atomic ensemble coupled to a band edge of a photonic crystal waveguide, New J. Phys. **19**, 083018 (2017).
[75] D. E. Chang, J. S. Douglas, A. González-Tudela, C.-L. Hung, and H. J. Kimble, Colloquium: Quantum matter built from nanoscopic lattices of atoms and photons, Rev. Mod. Phys. **90**, 031002 (2018).
[76] J. R. Johansson, G. Johansson, C. M. Wilson, and F. Nori, Dynamical Casimir Effect in a Superconducting Coplanar Waveguide, Phys. Rev. Lett. **103**, 147003 (2009).
[77] J. R. Johansson, G. Johansson, C. M. Wilson, and F. Nori, Dynamical Casimir effect in superconducting microwave circuits, Phys. Rev. A **82**, 052509 (2010).
[78] S. Pogorzalek, K. G. Fedorov, L. Zhong, J. Goetz, F. Wulschner, M. Fischer, P. Eder, E. Xie, K. Inomata, T. Yamamoto, Y. Nakamura, A. Marx, F. Deppe, and R. Gross, Hysteretic Flux Response and Nondegenerate Gain of Flux-Driven Josephson Parametric Amplifiers, Phys. Rev. Applied **8**, 024012 (2017).
[79] X. Wang, A. Miranowicz, and F. Nori, Ideal Quantum Nondemolition Readout of a Flux Qubit without Purcell Limitations, Phys. Rev. Applied **12**, 064037 (2019).
[80] See Supplemental Material at http://link.aps.org/supplemental/10.1103/PhysRevLett.126.043602 for detailed derivations of our main results, which includes Refs. [81–84].
[81] J. Q. You, X. Hu, S. Ashhab, and F. Nori, Low-decoherence flux qubit, Phys. Rev. B **75**, 140515(R) (2007).
[82] T. Ozawa, H. M. Price, A. Amo, N. Goldman, M. Hafezi, L. Lu, M. C. Rechtsman, D. Schuster, J. Simon, O. Zilberberg, and I. Carusotto, Topological photonics, Rev. Mod. Phys. **91**, 015006 (2019).
[83] S. Ryu, A. P. Schnyder, A. Furusaki, and A. W. W. Ludwig, Topological insulators and superconductors: Tenfold way and dimensional hierarchy, New J. Phys. **12**, 065010 (2010).
[84] C. L. Kane and T. C. Lubensky, Topological boundary modes in isostatic lattices, Nat. Phys. **10**, 39 (2014).
[85] W. Zhao and Z. Wang, Single-photon scattering and bound states in an atom-waveguide system with two or multiple coupling points, Phys. Rev. A **101**, 053855 (2020).
[86] C. Cohen-Tannoudji, J. Dupont-Roc, and G. Grynberg, *Atom–Photon Interactions* (Wiley, New York, 1998).
[87] A. González-Tudela and J. I. Cirac, Markovian and non-Markovian dynamics of quantum emitters coupled to two-dimensional structured reservoirs, Phys. Rev. A **96**, 043811 (2017).

[88] M. Lohse, C. Schweizer, O. Zilberberg, M. Aidelsburger, and I. Bloch, A Thouless quantum pump with ultracold bosonic atoms in an optical superlattice, Nat. Phys. **12**, 350 (2016).

[89] X. Gu, S. Chen, and Y.-X. Liu, Topological edge states and pumping in a chain of coupled superconducting qubits, arXiv:1711.06829.

[90] S. Nakajima, T. Tomita, S. Taie, T. Ichinose, H. Ozawa, L. Wang, M. Troyer, and Y. Takahashi, Topological Thouless pumping of ultracold fermions, Nat. Phys. **12**, 296 (2016).

[91] W. P. Su, J. R. Schrieffer, and A. J. Heeger, Solitons in Polyacetylene, Phys. Rev. Lett. **42**, 1698 (1979).

[92] M. Xiao, Z. Q. Zhang, and C. T. Chan, Surface Impedance and Bulk Band Geometric Phases in One-Dimensional Systems, Phys. Rev. X **4**, 021017 (2014).

[93] E. S. G. Naz, I. C. Fulga, L. B. Ma, O. G. Schmidt, and J. van den Brink, Topological phase transition in a stretchable photonic crystal, Phys. Rev. A **98**, 033830 (2018).